Non linear damping of a plate using Faraday instability of a fluid film

J.M. Génevaux, N. Dauchez, O. Doutres

Laboratoire d'Acoustique de l'Université du Maine, Avenue Olivier Messiaen, 72085 LE MANS Cedex 9

Abstract

Damping using an instability of a fluid film in contact with a vibrating structure is investigated. Waves induced in the fluid film is the source of the added damping. A model based on the theory of Faraday instability is applied to a clamped circular plate covered by a fluid film. It is shown that this original technique can provide a significant damping. It depends of the viscosity of the fluid, the local amplitude of the vibration, the threshold of the instability and the amplitude of the induced waves. The non linear relation between the amplitude of the waves and the plate acceleration induces a non linear damping. Theoretical and experimental results are compared. The model slightly overestimates the added damping. Comparison with viscoelastic and porous material treatments shows that damping are of the same order.

Key words: Thin films acoustical properties, Non linear acoustics, Mechanical waves resonance and damping, liquids viscosity, vibrations solid surfaces and interfaces, Vibroacoustics, Faraday instability

PACS: 68.60.B, 43.25, 46.40.F, 66.20, 68.35.J

1 Introduction

This paper examines a method to reduce the vibration and the emitted noise of a structure by mean of a fluid film in the low frequency range.

Usual techniques use a viscoelastic layer [1][2][3][4]. When bonded onto a structure, the viscoelastic layer is considered as undergoing a pure bending strain. Dissipation is proportional to the loss factor of the material and the flexural strain energy in the viscoelastic layer. This technique requires a sufficiently thick layer so that strain energy in the viscoelastic is significant compared to the strain energy of the base structure. To reduce the weight adding, a light and stiff constraining layer can be added: in this configuration, the viscoelastic layer undergoes shear strain and the thickness of the viscoelastic layer can be reduced. Optimal partially covering may also be used to reduce added mass [5]. Both techniques are limited by viscoelastic properties that are frequency and temperature dependent [6].

Usually used for sound absorbing, porous materials such as wool, fibre or polymer foam, may add significant damping when mounted onto a structure [7][8][9]. Below the first resonance frequency of the porous layer in its thickness, the porous layer acts as a viscoelastic layer undergoing flexural strain. Due to its higher thickness compared to those of the viscoelastic layers, its efficiency is limited by shear strain [9]. Around the thickness resonance, a high damping effect can be observed, but the acoustic radiation is amplified [7][8]. At higher frequencies the porous layer acts as a filter, that highly reduces the radiation of the structure.

To improve the efficiency of passive treatments, active control techniques have

been developed [10][11] but requires more sophisticated set up. Moreover, their robustness has to be carefully demonstrated.

In this paper, the presence of a fluid film in contact with a structure, can create a useful damping at low frequencies, due to wave generation at the fluid-air interface by Faraday instability (fig. 1). This technique can be compared with techniques using a distribution of small oscillators with or without low damping [12][13][14]. This instability appears when the normal acceleration of the wall in contact with the fluid film is strong enough [15][16]. In case of a finite area of the fluid-air interface, the boundary conditions select countable wave lengths and several stationary mode shapes are solution of the problem [17]. Several patterns of the fluid-air interface can occurs, but only the pattern which presents the smallest acceleration threshold appears [18]. The non-linear model of this parametric instability must take into account the dissipation in the fluid in order to evaluate the value of the acceleration threshold [19]. Experimental studies [17] confirm the threshold values and give the amplitude of the waves at saturation. For level of excitation far higher the threshold, the slow drift of the positions of the antinode of the fluid air interface can be explained by second order effects [20], and if the excitation is yet increased, ejection of droplets can be observed and modelled [21].

This paper focuses on the added dissipation to the structure by the Faraday instability, using the thinnest fluid layer without droplet ejections. To the author's knowledge, this technique to reduce the vibration using the Faraday instability was never presented.

In a first part (sec. 2), the modelling of the Faraday instability mechanism, its coupling with the vibrating structure and the method to calculate the added

damping is detailed. At this step, a geometrical configuration is chosen: a circular plate clamped at its edge.

In section 3, the corresponding experiment is designed in order to measure the added damping of the first mode of the plate. This highlight the non-linear behaviour of the instability of the fluid film and the influence of the parameters governing the phenomena and its coupling with the plate.

The results of the model are compared with those obtained by the experiment in section 4.

Finally a comparison with experimental results obtained on the same structure covered by porous material or a viscoelastic layer shows how effective the two techniques are (sec. 5).

2 Model

Faraday instability appears at the surface of a fluid subjected to normal oscillations. A model predicting the added damping by this phenomena on a plate is presented in this section. It is achieved in five steps that determine successively (fig. 2):

- 2.1) the wave length on the free surface,
- 2.2) the fluid damping ratio,
- 2.3) the damping coefficient of a fluid cell,
- 2.4) the local acceleration threshold, criterion for defining the area of instability and the amplitude of the waves,
- 2.5) the modal added damping coefficient, the modal stiffness, the modal

mass of the plate and the added damping ratio of the plate.

2.1 Calculation of the wave length on the free surface

2.1.1 Circular frequency of the free surface

For the Faraday instability which is a non linear phenomenon, a subharmonic circular frequency of the free surface at half the circular frequency of the excitation is obtained. This ratio between the two frequencies was not detected by Faraday in 1831 [15] who first observed the instability of free surfaces due to normal oscillations. For experiments using a single frequency excitation like ours [22] [23] [18], a model based on the hypothesis of inviscid fluid, slight displacement of the free surface and unwetting fluid, is given by Benjamin and Ursell [18]. In the case of the specific geometry of a gas bubble excited by an acoustic waves, Faraday instability is also present at the gas-fluid interface [24]. The finite area of the free surface induces that the stability, the increase of the waves and their saturation have been studied for countable wave lengths. This is not the case in this paper, due to the greatness of the ratio between the smallest length of the free surface and the concerned wave length: the side boundary conditions are so far that all the wave lengthes can be excited.

The free surface displacement $\xi(x, y, t)$ (fig. 1) is given by [18],

$$\xi(x, y, t) = AS(x, y) \exp(i\omega_f t) + c.c., \tag{1}$$

with $S(x, y)$ as the shape of the free surface, t the time and A the amplitude of the waves, ω_f the circular frequency of the free surface, and $c.c$ the complex conjugate of the first term. Benjamin and Ursell [18] show that the amplitude

equation of the waves is governed by a Mathieu equation,

$$\frac{\partial^2 A}{\partial t^2} + \omega_f^2 A - \tilde{\epsilon} g k \tanh(kh) \cos(\omega_e t) A = 0, \tag{2}$$

with $\tilde{\epsilon}$ the dimensionless acceleration of the bottom of the container, g the gravity, k the wave number of the free surface shape, h the thickness of the fluid layer and ω_e the circular frequency of the excitation. Douady [17] gives a dimensionless form of this equation,

$$\frac{\partial^2 \alpha}{\partial \tau^2} + (1 - \epsilon \cos(\tilde{r}\tau))\alpha = 0, \tag{3}$$

with $\alpha = A/h$, $\tau = t\omega_f$, $\tilde{r} = \omega_e/\omega_f$, and

$$\epsilon = \frac{\tilde{\epsilon}}{1 + \frac{\sigma k^2}{\rho_f g}}, \tag{4}$$

with σ the surface tension of the fluid-air interface and ρ_f the volumetric mass of the fluid.

Benjamin and Ursell [18] gave the stability chart of the solutions for Mathieu's equation, and equation (3) corresponds in their figure to $p = 1$ and

$$q = \frac{2k\epsilon g \tanh(kh)}{\omega_e^2}. \tag{5}$$

It appears that the half-frequency instability $\tilde{r} \simeq 2$ for $p = 1$ is obtained, and that no acceleration threshold is predicted by this model.

The first instability is thus given by,

$$\omega_f = \frac{\omega_e}{2}. \tag{6}$$

The frequency of the free surface is half the frequency of the excitation. This value of subharmonic comes from a local condition, so it does not depend on the geometry of the system [18][24]. This equation 6 will be considered in the

rest of the paper.

2.1.2 Wave number and wave length

The dispersion equation of free surface waves is given by [25] [26],

$$\omega_f^2 = gk \tanh(kh) \left(1 + \frac{\sigma k^2}{\rho_f g}\right). \tag{7}$$

In order to point out the influence of the surface tension over the gravity, it is written in the following form,

$$\omega_f^2 = \frac{2\pi g}{\lambda} \tanh\left(\frac{2\pi h}{\lambda}\right) \left(1 + \frac{4\pi^2 \sigma}{\rho_f \lambda^2 g}\right), \tag{8}$$

with $\lambda = 2\pi/k$ the wave length. The wave length of the free surface oscillations is given by solving eq. 8.

The term $\frac{4\pi^2\sigma}{\rho_f \lambda^2 g}$ is negligible before 1 below 20 Hz for water ($\sigma = 0.072$ N m^{-1}, $\rho_f = 1000$ kg m^{-3}): the gravity gives the rigidity of the free surface [26] [27] [28] [29]. The applicability of the method is restricted to horizontal free surfaces. Above 20 Hz, the surface tension plays the most important role. This paper is focused on this case of capillary waves. This damping method could be applied to a surface which is not horizontal. Note that in this case, an other type of instability due to the flow of the falling fluid film along a steady structure can occurs [30], but is not considered in this paper.

2.2 Type of damping in the fluid film

The damping due to the fluid film has three origins [31][32]: a) the surface layer, b) the viscous boundary layer at the interface with the structure and c) the dissipation due to the movement of the meniscus for a wetting fluid.

Mechanism c) which is strongly dependent of the cleanness of the contact line air-fluid-solid, is managed to be avoided: the plate is clamped at its boundaries and the dimensions of the plate are chosen far greater than the wave length λ. In this context, the waves are avoided in the vicinity of the meniscus.

Mechanism b) is not considered in this study. The chosen flow field in a fluid cell is approximated by a potential flow. The thickness of the viscous skin is neglected.

Only mechanism a) is considered. The damping of the free surface waves is given by the logarithmic decrement [19]:

$$\alpha_s = 2\pi\delta k, \tag{9}$$

with $\delta = \sqrt{2\nu/\omega_f}$ as the thickness of the viscous layer for a fluid with a kinematic viscosity ν solicited at the circular frequency ω_f.

2.3 Calculation of the equivalent damping coefficient of a fluid cell

The aim of this section is to calculate the modal damping coefficient $\hat{c}$ of the fluid per unit area. It is given by,

$$\hat{c}(r,\theta) = 2\zeta_0 m_f \omega_f, \tag{10}$$

with m_f the modal mass per unit area and ζ_0 the damping ratio of the fluid. ζ_0 can be related to the logarithmic decrement α_s (eq. 9) of free oscillations [33] by,

$$\zeta_0 = \frac{\alpha_s}{\sqrt{4\pi^2 + \alpha_s^2}}. \tag{11}$$

The modal mass par unit area m_f is derived from m_{fcell} the modal mass of

one cell whose area is $(\lambda/2)^2$,

$$m_f = \frac{m_{fcell}}{(\lambda/2)^2}. \tag{12}$$

Indeed, the first mode of a fluid cell for a given pattern of the free surface is considered. The literature theories of Faraday instability show that several pattern (roll, square, hexagon) can be present on the free surface if a single frequency composes the excitation [16]. In this paper, the square pattern is chosen to develop the model (see fig. 7). The modal shape can be defined according to a potential function for the flow. Let us consider a fluid cell defined by a volume of incompressible fluid, whose lengthes are $\lambda/2$ in $\mathbf{x}$ and $\mathbf{y}$ directions, and a depth h in direction $\mathbf{z}$ (fig. 3). Symmetry arguments allow the use of a flow $\mathbf{v}$ relative to the plate associated to $\Phi_f(x,y,z,t) = \phi_f(x,y,z)(-\omega_f \sin \omega_f t)$, as,

$$\phi_f(x,y,z) = \beta(r,\theta)\cos(q(2x/\lambda - 1))\cos(q(2y/\lambda - 1))\cosh(\sqrt{2}qz/\lambda), \tag{13}$$

with β the amplitude of the potential function which depends of the position of the fluid cell (cylindrical coordinates r,θ), and (x,y,z) the coordinates of a point into the cell. The velocity field $\mathbf{v}$ is given by,

$$h\frac{\partial \phi_f}{\partial x}(-\omega \sin \omega_f t) = \mathbf{v}.\mathbf{x}, \tag{14}$$

$$h\frac{\partial \phi_f}{\partial y}(-\omega \sin \omega_f t) = \mathbf{v}.\mathbf{y}, \tag{15}$$

$$h\frac{\partial \phi_f}{\partial z}(-\omega \sin \omega_f t) = \mathbf{v}.\mathbf{z}. \tag{16}$$

The boundary conditions at $x = \lambda/2$ and $y = \lambda/2$ give,

$$q = n\pi. \tag{17}$$

The value $n = 1$ corresponds to the first mode.

The kinetic energy of the fluid in the cell is used to calculate m_{fcell}:

$$\begin{aligned} &\tfrac{1}{2} m_{fcell} \left(\tfrac{\partial \alpha(r,\theta) \cos(\omega_f t)}{\partial t} \right)^2 = \\ &\qquad \tfrac{1}{2} \rho_f (-\omega_f \sin(\omega_f t))^2 \int_{x=0}^{\lambda} \int_{y=0}^{\lambda} \int_{z=0}^{h} \left(\phi_{f,x}^2 + \phi_{f,y}^2 + \phi_{f,z}^2 \right) dxdydz, \end{aligned} \tag{18}$$

with $\alpha(r,\theta)$ as the dimensionless amplitude of the wave and $\phi_{f,x} = \frac{\partial f}{\partial x}$. The equality of the vertical velocity of a point of the free surface ($z = h$) gives the relation between $\alpha(r,\theta)$ and $\beta(r,\theta)$:

$$\alpha(r,\theta) \frac{\partial \cos(\omega_f t)}{\partial t} = (-\omega \sin(\omega_f t)) \frac{\partial \phi_f}{\partial z}, \tag{19}$$

$$\alpha(r,\theta)(-\omega_f \sin(\omega_f t)) = \beta(r,\theta)(-\omega_f \sin(\omega_f t)) \frac{2\sqrt{2}\pi}{\lambda} \sinh(\sqrt{2}\pi h/\lambda), \tag{20}$$

so that,

$$\beta(r,\theta) = \frac{\alpha(r,\theta)\lambda}{2\sqrt{2}\pi \sinh(\sqrt{2}\pi h/\lambda)}. \tag{21}$$

Using 21, and integrating the second member of equations 18, the modal mass of the 1 degree of freedom system associated to the fluid cell is,

$$m_{fcell} = \frac{\rho_f \lambda^3 \sqrt{2}}{256\pi} \frac{\left(1 - \exp\left(\frac{-8\sqrt{2}\pi h}{\lambda}\right)\right) \exp\left(\frac{4\sqrt{2}\pi h}{\lambda}\right)}{\cosh\left(\frac{\sqrt{2}\pi h}{\lambda}\right)^2 - 1}. \tag{22}$$

The modal mass per unit area m_f (eq. 12) and the modal damping coefficient by unit area (eq. 10) are finally obtained.

2.4 Calculation of the local acceleration threshold, the amplification of the waves, and the instability domain

The dissipation is added on the structure only in the area in which the instability is present. A local hypothesis is assumed: the amplitude of the waves of a fluid cell at a point depends solely on the amplitude of the acceleration of

this point. This need to determine the local acceleration of the plate, and the relation between this acceleration to get the amplitude of the waves.

2.4.1 Amplitude of the induced waves

In this section a model to determine the amplitude of the waves at saturation is presented.

In the case of a spatially uniform excitation of the fluid film, Douady [17] gives the amplification rate of the waves as a function of ϵ the excitation and $\bar{A}$ is the complex conjugate of A the amplitude of the wave,

$$\frac{\partial A}{\partial t} = \gamma \exp(i\phi)A + \frac{\epsilon\omega_f}{4}\bar{A} + c\exp(i\psi)|A|^2 A, \tag{23}$$

with γ the acceleration. The amplitude at saturation, when $\frac{\partial A}{\partial t} = 0$, is an affine function of $\tilde{\epsilon} = \gamma/g$,

$$\alpha^2 = \tilde{\epsilon} A_{\omega_f} - B_{\omega_f}, \tag{24}$$

where A_{ω_f} and B_{ω_f} are two parameters which will be determined experimentally in this paper (sec. 4.2 and fig. 12).

2.4.2 Definition of the local threshold

Because of the dissipation in the fluid cell, a phenomenological damping term is added in the equation 3 [17],

$$\frac{\partial^2 \alpha}{\partial \tau^2} + (1 - \epsilon\cos(r\tau))\alpha + 2\eta\frac{\partial \alpha}{\partial \tau} = 0. \tag{25}$$

The evaluation of η can be found in [19] and [34] for a theoretical approach and in [17] for an experimental approach. This induces a threshold beyond

which surface waves are observed.

Several threshold values can be found in the literature.

- For capillary waves, deep water, and inviscid fluids, Milner [19] gives a threshold for the first half-frequency instability which is

$$\tilde{\epsilon}_{c1} = \frac{1}{g} 8 \omega_f k \nu. \tag{26}$$

- With a hypothesis of low viscosity, the dissipation can be calculated according to the inviscid flow field and gives a second estimation of the threshold [35]

$$\tilde{\epsilon}_{c2} = \frac{1}{g} 8 (\rho_f / \sigma)^{1/3} \nu \omega_f^{5/3}, \tag{27}$$

  which is a little higher than the evaluation of Milner [19].

The comparison with the experimental thresholds obtained by Douady [17] are in good agreement with both models which are very close to each other. Nevertheless, two hypothesis of the preceding models are not verified in our case and may affect the threshold:

- the acceleration of the structure is not uniform,
- the depth of the fluid film is not infinite, and this may increase the threshold due to dissipation at the bottom of the fluid domain.

Consequently, an approximation of the threshold will be determine posing $\alpha = 0$ in the equation 24. It can be written as a function of the measured values of A_{ω_f} and B_{ω_f},

$$\tilde{\epsilon}_c = \frac{B_{\omega_f}}{A_{\omega_f}}. \tag{28}$$

2.4.3 Local hypothesis

The hypothesis of a local reacting behaviour is assumed: the amplitude of the waves of a fluid cell at a point $P(r,\theta)$ depends solely on the amplitude $W_a(r,\theta)$ of the acceleration of the corresponding point of the plate $\ddot{w}(r,\theta,t) = W_a(r,\theta)\sin(\omega_e t)$. The amplitude of the waves does not depend on the acceleration of the other points on the plate.

The dimensionless amplitudes of the waves α at each point of the plate must verify $0 \leq \alpha \leq 1$. Using equation (24), according to the acceleration at a given point:

- $W_a(r,\theta)) \leq \tilde{\epsilon}_c g$, no waves below this value,
- $\tilde{\epsilon}_c g \leq W_a(r,\theta)) \leq g\frac{1+B_{\omega_f}}{A_{\omega_f}}$, waves are present between these values,
- $g\frac{1+B_{\omega_f}}{A_{\omega_f}} \leq W_a(r,\theta))$, the model is not valid above this value.

2.5 Calculation of equivalent modal dissipation, stiffness and mass of the plate and added damping ratio

This section describes the procedure to calculate the added damping ratio of the plate. The area of fluid instability depends on the shape of the displacement of the plate at the excitation frequency and the amplitude of excitation. In the present paper, the response of a circular clamped plate of diameter d (sec. 3.1) near its first mode is considered. The first mode shape of the plate is given by [33],

$$\phi(r,\theta) = \frac{I_0(\beta_{01}d/2)\, J_0(\beta_{01}r) - J_0(\beta_{01}d/2)\, I_0(\beta_{01}r)}{I_0(\beta_{01}d/2)\, J_0(0) - J_0(\beta_{01}d/2)\, I_0(0)}, \tag{29}$$

with I_0 as the modified Bessel function, J_0 the Bessel function and $\beta_{01} = 1.015\frac{2\pi}{d}$ (fig. 6). This mode shape is normalized so that $\phi(0,0) = 1$.

The equivalent damping ratio added to the plate ζ_{ap} is given by,

$$\zeta_{ap} = \frac{c_{ap}}{2\sqrt{k_p m_{pf}}}, \tag{30}$$

with c_{ap} as the added damping coefficient on the plate, k_p the modal stiffness of the plate and m_{pf} the modal mass of the plate loaded by the fluid film.

This three terms c_{ap}, k_p and m_{pf} are calculated in the following sections. The comparison between theoretical and experimental values (sec. 3) of ζ_{ap} will be presented in section 4.

2.5.1 Added damping coefficient

The added damping coefficient c_{ap} is related to the modal shape $\phi(r,\theta)$ of the plate, the local damping coefficient per unit area $\hat{c}$ and the amplitude of the waves $\alpha(r,\theta)$ (eq. 24):

$$\int_{t=0}^{2\pi/\omega_e} \frac{1}{2} c_{ap} \dot{w}^2(0,0,t) dt = \int_{t=0}^{2\pi/\omega_e} \left[\frac{1}{2} \int_{\theta=0}^{2\pi} \int_{r=0}^{R} \hat{c} \left(\frac{\partial h \alpha(r,\theta) \cos(\omega_f t)}{\partial t} \right)^2 r dr d\theta \right] dt. \tag{31}$$

Taking into account the axisymmetry of the first mode shape, that $\omega_f = \omega_e/2$ (eq. 6) and $\dot{w}(0,0,t) = W(0,0)\omega_e \sin(\omega_e t)$, the integration in time and in angle θ gives,

$$c_{ap} W(0,0)^2 = \hat{c} h^2 \pi \int_{r=0}^{R} \alpha(r)^2 r dr. \tag{32}$$

Introducing r_d as the radius at which the instability appears,

$$\ddot{w}(r_d,\theta) = \tilde{\epsilon}_c g, \tag{33}$$

the local hypothesis gives that $\alpha(r) = 0$ for $r > rd$, and equation 24 for $r < r_d$ becomes:

$$c_{ap} = \frac{\pi \hat{c} h^2}{W(0,0)^2} \left[A_{\omega_f} g \int_{r=0}^{r_d} \tilde{\epsilon}(r) r dr - B_{\omega_f} \int_{r=0}^{r_d} r dr \right]. \tag{34}$$

The dimensionless acceleration $\tilde{\epsilon}(r)$ can be related to $\phi(r)$ the normalized mode shape of the plate (eq. 29),

$$\tilde{\epsilon} = \frac{W(0,0)\omega^2}{g} \phi(r,\theta). \tag{35}$$

The evolution of c_{ap} can then be calculated according to the value of $W(0,0)\omega^2$.

2.5.2 Modal stiffness

The strain energy of the plate is calculated by integrating the local strain energy over the plate. This expression gives the modal stiffness k_p [33]:

$$\frac{1}{2} k_p \left(\phi(0,0)\right)^2 = \frac{1}{2} D \int_{\theta=0}^{2\pi} \int_{r=0}^{R} \left(\left(\phi_{,rr} + \frac{1}{r} \phi_{,r} \right)^2 - 2(1-\nu_p) \frac{\phi_{,rr} \phi_{,r}}{r} \right) r dr d\theta, \tag{36}$$

with $D = Ee^3/(2(1-\nu_p^2))$ the stiffness of the plate. This modal stiffness does not depend on the fluid film properties.

2.5.3 Modal mass

By the same approach for the kinetic energy of the plate, the modal mass of the plate m_p is given by [33]:

$$\frac{1}{2} m_p \left(\phi(0,0)\right)^2 = \frac{1}{2} \int_{\theta=0}^{2\pi} \int_{r=0}^{R} \rho_p e \phi(r,\theta)^2 r dr d\theta. \tag{37}$$

With,

$$\rho_p = \frac{\rho_s e + \rho_f h}{e} = \rho_s(1 + \tilde{\rho}), \tag{38}$$

the equivalent volumetric mass of the system, based on ρ_s the volumetric mass of the aluminum and an added mass due to the fluid layer. Assuming that ρ_p is constant along the plate and that $\phi(0,0) = 1$, equation 37 can be rewritten,

$$m_p = \rho_p e \int_{\theta=0}^{2\pi} \int_{r=0}^{R} \phi(r,\theta)^2 r dr d\theta. \tag{39}$$

3 Experimental results

The aim of this section is to quantify experimentally the energy dissipation induced by a Faraday instability of a heavy fluid film. Because the system is non linear, all experimental quantities are referenced to the acceleration at the center of the plate which is given for each figure.

3.1 Experimental set-up

The geometrical configuration is presented in figure 4. A circular aluminum plate of diameter $d = 0.290$ m is clamped. Its characteristics are summarized in table 1. It is excited by a shaker connected to its centre via a force transducer giving the excitation force F. An accelerometer of mass $m_a = 0.0042$ kg is bonded at 1 cm of the center of the plate to get the reference acceleration $W_a(0,0)$. A laser vibrometer is focused on the plate through the fluid film.

The frequency range is set between 40 Hz and 120 Hz to ensure Faraday instabilities for reasonable accelerations. The thickness of the fluid layer is chosen to be of the order of the wavelength: this ensures a total covering of

the plate and a small added mass.

Between each test using different fluids, the container is cleaned up and dried. The frequency response functions are obtained using a step by step harmonic excitation for a controlled acceleration amplitude $W_a(0,0)$.

3.2 Determination of the free surface velocity of the fluid

The signal given by the laser vibrometer is proportional to the apparent velocity of the plate $\frac{d\tilde{w}}{dt}$, which is a combination of the plate and the free surface velocities.

$$\frac{d\tilde{w}(r,\theta,t)}{dt} = \frac{dw(r,\theta,t)}{dt} - \left(\frac{c_0}{c_1} - 1\right)\frac{dh(r,\theta,t)}{dt}, \tag{40}$$

with $w(r,\theta,t)$ the displacement of the plate at the point $P(r,\theta)$, c_0 the light velocity in the air, c_1 the light velocity in the fluid, $h(r,\theta,t)$ the water level crossed by the beam. Their contributions can be easily identified because they are at different frequencies. To do so, equation 40 is rewritten of the form:

$$\frac{d\tilde{w}(r,\theta,t)}{dt} = \tilde{a}_1\cos(\omega_e t + \tilde{a}_2) + \tilde{a}_3\cos\left(\frac{\omega_e}{2}t + \tilde{a}_4\right). \tag{41}$$

The parameters $\tilde{a}_1$ and $\tilde{a}_2$ are associated to the plate velocity, and the parameters $\tilde{a}_3$ and $\tilde{a}_4$ to the fluid interface movement. They are determined using a non linear optimisation. The position of the nodes of the free surface mode shape are not stationary: $\tilde{a}_3 = 0$ if the laser beam focuses through a node, and is maximum if the laser beam focuses through an antinode. Thus, several identifications must be pursued on different times, and only the greatest value of $\tilde{a}_3$ must be considered to calculate the amplitude of the waves.

3.3 Influence of the parameters

The influence of the following parameters are tested successively: the fluid level, the amplitude of excitation and the viscosity of the fluid.

Bare plate

First, a reference experiment without fluid is performed. The frequency response function (accelerance) is shown in continuous line figure 5. The resonance corresponds to the first mode of the plate. Figure 6 shows a good agreement between the theoretical and experimental mode shapes.

An added mass effect

The following experiments are performed with water to test the influence of the fluid level on the frequency response functions. The water levels remain under 0.016 m for all the experiments described. The ratio of added mass per unit area is:

$$\tilde{\rho} = \frac{\rho_f h}{\rho_s e}. \tag{42}$$

As the water level increases (fig. 5):

- the resonance frequency decreases,
- the amplitude of the peak decreases: this not only due to the added mass but also to the added damping as presented in section 4.
- near the resonance frequency, stationary waves are observed on the free surface (fig. 7). Their wavelength (0.005 m) increases as the frequency decreases. This length is consistent with capillarity waves on the surface. They

appear as square patterns within a circle at the center of the plate. Their amplitude is higher at the center of the plate. This coincides with the maximum amplitude of the first mode shape.

The excitation threshold for Faraday instability

The frequency response function is measured for several amplitude of the excitation for water levels from 0 to 0.0133 m. Non-linear effects are observed (fig. 8):

- a slight increase in the frequency resonance according to the amplitude of excitation,
- a reduction of the amplitude of the peak (-13 dB),
- an increase in the circular surface on which waves are present according to the excitation,
- the time signal of the apparent speed of the plate (fig. 10) exhibits a subharmonic at $\omega_e/2$.
- the existence of a threshold for waves to appear. In figure 8, the threshold is between 6 m s^{-2} and 13 m s^{-2}. It corresponds to a sharp increase in damping. Figure 9 shows damping estimated using the half-power method according to the acceleration level. This increase is not observed for the bare plate (continuous line). The thinner the fluid layer, the stronger the damping is.

The effect of viscosity on the acceleration threshold

At a given acceleration, an increase of the viscosity of the fluid do not necessary induces a higher dissipation. To reveal this fact, the water is replaced by oil with a much higher viscosity. The amplitude of the excitation (16.75 m s^{-2}) is chosen such that the waves appear with water but not with oil: this indicates that the excitation threshold for oil is higher than for water. Moreover, figure 11 shows that the amplitude of the maximum of the frequency response is 10 dB higher than the amplitude with water. Indeed, the viscosity is so strong that no local relative fluid velocity appears between the oil and the plate: its viscosity does not contribute to the frequency response of the system, but only its mass. For water both effects of viscosity and added mass are observed (fig. 5).

4 Comparison between the model and the experimental results

The coherence between the experimental and theoretical values of the dissipation induced by a heavy fluid film on the surface of a vibrating structure is now evaluated. The numerical values of the parameters of the model will be given along this section for one specific configuration.

4.1 Stiffness of the bare plate and equivalent mass per unit area of the plate

The apparent stiffness of the plate D and the equivalent volumetric mass of the plate is determined from the frequencies of the first resonance of the plate without and with the fluid layer (fig. 5) by $f_1 = \frac{1.015^2}{2\pi}\frac{\pi^2}{(d/2)^2}\sqrt{\frac{D}{\rho_s e(1+\tilde{\rho})}}$ giving

$D = 8.82$ N m and $\rho_s = 5230$ kg m^{-3}.

4.2 Instability threshold, circular frequency and wave height of the free surface

The instability threshold and the wave height of the free surface measured during experiments, are compared to the modelled one's. The frequency of the excitation is chosen near the first resonance of the coupled system at 75 Hz with a water level of $h = 0.0046$ m.

The experimental threshold, which is between 6 ms^{-2} and 13 ms^{-2} (fig. 9), is significantly greater than the theoretical one's (eq. 26, 27): $\tilde{\epsilon}_{c1}\, g = 2.99$ ms^{-2}, $\tilde{\epsilon}_{c2}\, g = 1.73$ ms^{-2}. This can be attributed to the small ratio between the wave length and the fluid layer thickness (effect of finite depth), or to the fact that the amplitudes of acceleration is not uniform. Above the experimental threshold, the circular frequency of the free surface is half the circular frequency of the plate, as predicted by the model of the Faraday instability. The two frequencies $\omega_e = 2\pi 75$ s^{-1} and $\omega_f = \omega_e/2 = \pi 75$ s^{-1} are present in the signal corresponding to the apparent velocity of the plate if the instability occurs (fig. 10).

The identification of the coefficients A_{ω_f} and B_{ω_f} (eq. 24) are determined from experimental datas by a least-squares regression method (fig. 12). The uncertainties on the position of the regression line are calculated with a confidence of 95%. Note that three points are not taking into account: the noise on the signal and the low spatial stability of the waves do not permit to correctly evaluate the amplitude of the waves for these three acceleration levels.

The identified values in equation 24 are:

- $0.0135 < A_{\omega_f} < 0.0163$,
- $0.0111 < B_{\omega_f} < 0.0134$,
- $\tilde{\epsilon_c} g = 8.04$ ms^{-2}.

In the following, above the threshold $\tilde{\epsilon}_c = 8.04/9.81 = 0.82$, the dimensionless amplitudes of the waves lye in the following boundaries:

$$0.0135(\tilde{\epsilon} - 0.82) < \alpha^2 < 0.0163(\tilde{\epsilon} - 0.82). \tag{43}$$

The wave length $\lambda = 0.004$ m given by the model (eq. 7) with $\sigma = 0.072$ N m^{-1} and $g = 9.81$ m s^{-2}, is coherent with the estimation of the experimental wave length ($\lambda = 0.005$ m, sec. 3.3).

4.3 Added damping

4.3.1 Damping ratio of the fluid

The local dissipation due to the oscillation of the free surface is given by equation 11: $\zeta_0 = 14.5\%$ for water with $\nu = 10^{-6}$ m^{2}s^{-1}, $\delta = \sqrt{2\,10^{-6}/(\pi 75)} = 9.21\,10^{-5}$ m and $\alpha_s = 0.919$.

4.3.2 Damping coefficient of the fluid per unit area

The preceding dissipation will act strongly or not, according to the considered movement in a fluid cell. Considering the pre-defined values of λ, g, ω_f, σ, ρ_f, equation 22 gives: $m_{fcell} = 5.45\,10^{-10}$ kg which represents a small part of the mass of the considered fluid cell. Equation 12 gives $m_f = 1.39\,10^{-4}$ kg m^{-2}

and the equivalent damping coefficient per unit area $\hat{c} = 9.49$ kg m^{-2}s^{-1} (eq. 10).

4.3.3 Added damping ratio from the fluid on the plate

The equivalent damping coefficient c_{ap} added to the structure depends on the area on which the damping occurs and the amplitude of the waves. The first mode shape of the plate induces a circular limit of instability of radius r_d where,

$$W_a(r_d, \theta) = 8.04 \text{ m s}^{-2}. \tag{44}$$

The relationship (fig. 13) between this radius and the acceleration in the center of the plate is given by the mode shape of the plate $\phi(r, \theta)$ (eq. 29) and the instability threshold (eq. 44). The evolution of c_{ap} as function of $W_a(0, 0)$ can then be calculated and is plotted figure 14 taking into account the uncertainty of the amplitude of the waves (eq. 43).

According to the values of the parameters of the plate, the modal stiffness is $k_p = 1.08\,10^5$ N m^{-1} (eq. 36), the equivalent mass of the plate with fluid is $\rho_p = 7215$ kg m^{-3} (eq. 38) and the modal mass is $m_p = 0.0875$ kg (eq. 39).

The evolution of c_{ap}, the damping ratio added by the fluid ζ_{ap} (eq. 30) can be plotted (fig. 15).

For the experimental point of view, the damping ratio added by the fluid can be deduced by the comparison of the damping ratio observed with the fluid ζ_{pf} and the damping ratio of the bare plate ζ_p (fig. 9). The damping ratio of

the bare plate is,

$$\zeta_p = \frac{c_p}{2\sqrt{k_p m_p}}, \tag{45}$$

with c_p the modal damping coefficient of the plate, m_p the modal mass of the plate. With the fluid layer the damping ratio is given by,

$$\zeta_{pf} = \frac{c_p + c_{ap}}{2\sqrt{k_p m_{pf}}} = \frac{c_p}{2\sqrt{k_p m_{pf}}} + \zeta_{ap}. \tag{46}$$

By neglecting the kinetic energy of the waves compared to the kinetic energy of the loaded plate, the relation $m_{pf} = m_p(1 + \tilde{\rho})$ gives,

$$\zeta_{pf} = \frac{c_p}{2\sqrt{k_p m_p(1 + \tilde{\rho})}} + \zeta_{ap}. \tag{47}$$

Thus, the experimental value of the added damping ratio is

$$\zeta_{ap} = \zeta_{pf} - \zeta_p \frac{1}{\sqrt{1 + \tilde{\rho}}}. \tag{48}$$

The comparison (fig. 15) between experimental and theoretical values of ζ_{ap} shows that:

- an increase of the damping beyond the threshold is observed,
- the amplitude of the theoretical damping is of the same order but greater than the experimental damping.

In fact, the model is strongly sensitive of the amplitude of waves. The relation between the wave amplitude and the acceleration has been determined assuming a locally reacting behaviour of each fluid cell. This hypothesis is valid where the acceleration is uniform: this is the case in the vicinity of an antinode (center of the plate for the first mode). This assumption may not be valid where an acceleration gradient is present. Moreover in this transition region, the cell shape is no more square (fig. 7).

5 Dissipation efficiency for porous, viscoelastic and fluid film treatments

The same circular plate is tested with a viscoelastic treatment and with porous materials.

A 2 mm thick viscoelastic layer is bonded on the whole plate. This treatment induces an added mass of 0.309 kg to the plate : $\tilde{\rho} = 0.90$. The damping ratio measured is approximately 4.5% and is independent of the amplitude of the excitation (fig. 16).

Two sound absorbing polymer foam are also tested. Their acoustical and mechanical parameters according to Biot-Allard [7] theory are given in table 2. It should be noted that the Young Modulus reported and the loss factor of the skeleton were determined at 5 Hz using quasistatic measurement. A slight added mass effect is observed when a layer is added. The damping is also plotted in figure 16. The porous treatments induce slight increases in damping compared to that obtained for the bare plate. As for the viscoelastic layer, this added damping appears largely unrelated to the level of excitation.

Compared to these usual materials, the damping induced by the fluid layer with $\tilde{\rho} = 0.88$, is strongly non linear, and may be significant in comparison with other treatments.

6 Conclusion

Damping of a vibrating structure by mean of a heavy fluid film subjected to Faraday instability as been studied. It is shown that added damping may be

not negligible. The presence of an heavy fluid film on the surface of a vibrating structure induces a non negligible dissipation of energy due to Faraday instability. A model has highlighted the governing parameters: the acceleration threshold and the amplitude of the waves, which depend on the frequency, the viscosity and the fluid thickness ; the mode shape of the structure. The model takes into account that the dissipation do not act on the overall structure. Experimental results has confirmed the tendencies and the order of the predicted damping.

Nevertheless, this dissipation predicted by the model is slightly overestimated. Further experiments are needed to detect the sources of discrepancies: the Faraday instability threshold and the amplitude of the waves must be studied in the case of non uniform excitation.

ACKNOWLEDGMENTS

Thanks to Lazhar Benyahia from the Laboratoire Polyméres, Colloides, Interfaces of the Université du Maine (Le Mans, France) for our productive discussions. Thanks to Susanna Wesson and Denis Ritter for the English corrections.

References

[1] A.D. Nashif, D.I.G. Jones, J.P. Henderson, *Vibrations damping*, J. Wiley & sons, 1985

[2] D. Ross, E.E. Ungar, Jr E.M. Kerwin *Structural Damping ; Damping of plate flexural vibrations by means of viscoelastic laminate*, ASME, New-York, pp49-88. 1959

[3] ASTM E756-98, Standard Test Method for Measuring Vibration-Damping Properties of Materials: Oberst bar

[4] L. Beranek, *Noise and vibration control*, Institute of Noise Control Engineering, Washingtown, USA, 1988 The Journal of the Acoustical Society of America, **83**, 3, pp. 1206-1207, 1988

[5] M. Alvelid, *Optimal position and shape of applied damping material* Journal of Sound and Vibration **310** pp 947-965, 2008

[6] T. PRITZ, *Loses factor peak of viscoelastic materials : magnitude to width relations* Journal of Sound and Vibration, **246**,2, pp265-280, 2001

[7] 0. Doutres, N. Dauchez, J.M. Génevaux, *Validity of the limp model for porous materials: A criterion based on Biot theory*, J of Acoustical Society of America **122**, pp2038-2048, 2007

[8] 0. Doutres, N. Dauchez, J.M. Génevaux, *Porous layer impedance applied to a moving wall : Application to the radiation of a covered piston*, J of Acoustical Society of America **121**,1, pp206-213, 2007

[9] N. Dauchez, S. Sahraoui, N. Atalla, *Investigation and modelling of damping in a plate with a bonded porous layer*, Journal of Sound and Vibration, **265**,2 , pp437-449, 2003

[10] A. Baz, *Robust control of active constrained layer damping*, Journal of Sound and Vibration, **211**, 3, pp467-480, 1998

[11] D. Guyomar, A. Badel, *Nonlinear semi-passive multimodal vibration damping: An efficient probabilistic approach* Journal of Sound and Vibration, **294**,1-2, pp249-268, 2006

[12] R.J. Nagem, I. Veljkovic, G. Sandri, *Vibration damping by continuous distribution of undamped oscillators*, Journal of Sound and Vibration, **207**,3, pp429-434, 1997

[13] M. Strasberg, D. Feit, *Vibration damping of large structures induced by attached small resonant structures*, J. Acoust. Soc. Am. **99**, pp335, 1996

[14] D.J. Thompson, *A continuous damped vibration absorber to reduce broad-band wave propagation in beams*, Journal of Sound and Vibration **311** pp824-842, 2008

[15] L. Faraday, *On the forms and states of fluids on vibrating elastic surfaces*, Philos. Trans. Royal Inst., London, **121**, p229, 1831

[16] A. V. Kityk, K. Knorr, H.-W. Muller and C. Wagner, *Spatio-temporal Fourier analysis, of Faraday surface wave patterns on a two-liquid interface*, Europhysics letter **65**,6, pp857-863, 2004

[17] S. Douady, *Experimental study of the Faraday instability*, J. of Fluid Mech., **221**, pp383-409, 1990

[18] T.B. Benjamin, F. Ursell, *The stability of the plane free surface of a liquid in vertical periodic motion* Proc Royal Soc. of London, A, **225**, pp505-515, 1934

[19] S.T. Milner, *Square patterns and secondary instabilities in driven capillary waves*, J. Fluid Mech., **225**, p81-100, 1991

[20] E. Martin, C. Martel, J.M. Vega, *Drift instability of standing Faraday waves* Journal of Fluid Mechanics **467**, pp57-79, 2002

[21] S. Alzuaga, J.-F. Manceau, F. Bastien *Motion of droplets on solid surface using acoustic radiation pressure* Journal of Sound and Vibration, **282**, pp151-162, 2005

[22] L. Matthiessen, Ann. Phys., Lpz., **141**, p375, 1870

[23] L. Rayleigh, *On the crispation of fluid resting upon a vibrating support.* Phil. Mag. **5**,5, pp50-58, 1883

[24] A.O. Maksimov, T.G. Leighton, *Transient processes near the threshold of acoustically driven bubble shape oscillations*, Acta Acustica, 87(3), 2001, 322-32

[25] H. Lamb *Hydrodynamics* (6th ed.), Cambridge University Press, 1994

[26] J.M. Génevaux,X.J. Chai, J.P. Brancher, *Gravity effects on coupled frequencies of a 2D fluid-structure problem with free surface*, J. of Sound and Vibrations, **215**,2, pp331-342, 1998

[27] J. Kyeong-Hoon, L. Semg-Cheol, *Fourier series expansion method for free vibration analysis of either a partially liquid-filled or a partially liquid-surrounded circular cylindrical shell*, Computers and Structures **58**,5, pp931-946, 1995

[28] M. Amabili, M.P. Paidoussis, A.A. Lakis, *Vibration of partially filled cylindrical tanks with ring-stiffeners and flexible bottom*, J. of Sound and Vibrations, **213**,2, pp259-299, 1998

[29] Y.K. Cheung, D. Zhou, *Hydroelastic vibration of a circular container bottom plate using the Galerkin method*, J. of Fluids and Structures,**16**,4, pp561-580, 2002

[30] W. Ambrosini, N. Forgione, F. Oriolo, *Statistical characteristics of a water film falling down a flat plate at different inclinations and temperatures*, International Journal of Multiphase Flow, **28**,9, pp1521-1540, 2002

[31] J.W. Miles, *Parametrically excited solitary waves* J. of Fluid Mechanics, **148**, pp451-460, 1984

[32] J.W. Miles, *Surface-wave damping in closed basins.* Proc. of the Royal Soc. London, A **297**, pp459-475, 1967

[33] M. Geradin, D. Rixen, *Théorie des vibrations : application à la dynamique des structures* Masson, Paris, 1993

[34] W.S. Edwards, S. Fauve *Parametrically excited quasicrystalline surface waves* Physical Review E, **47**,2, pp788-791, 1993

[35] W.S. Edwards, S. Fauve, *Patterns and quasi-patterns in the Faraday experiment* J Fluid Mech., **278**, pp123-148, 1994

List of Figures

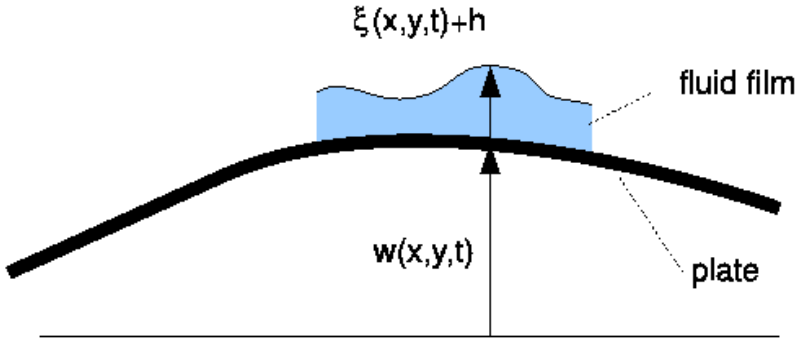

Fig. 1. Oscillation of a fluid film on a vibrating plate.

.

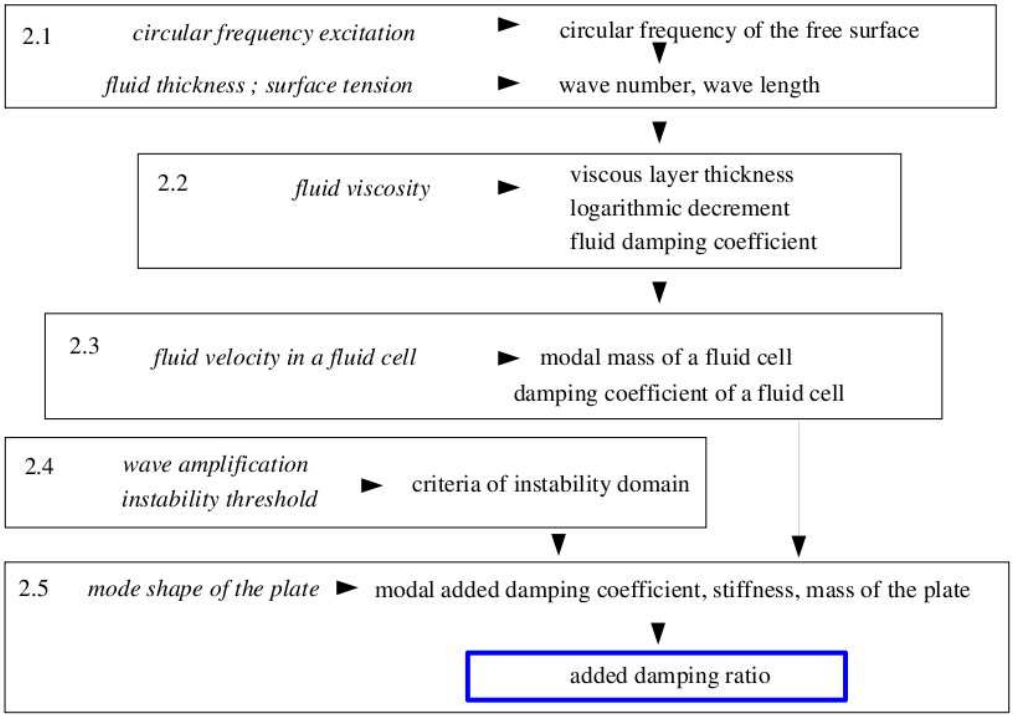

Fig. 2. Synopsis of the model construction.

.

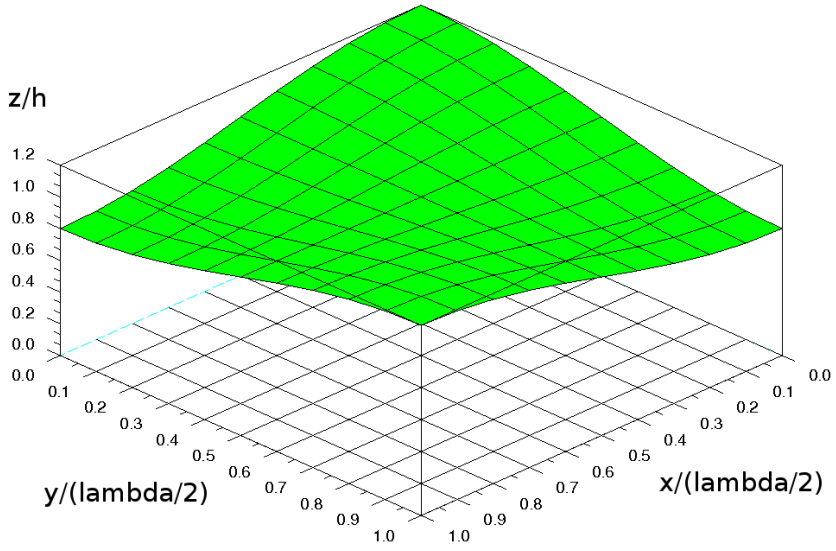

Fig. 3. The oscillation pattern of the fluid in a cell excited at its bottom by the plate.

.

.

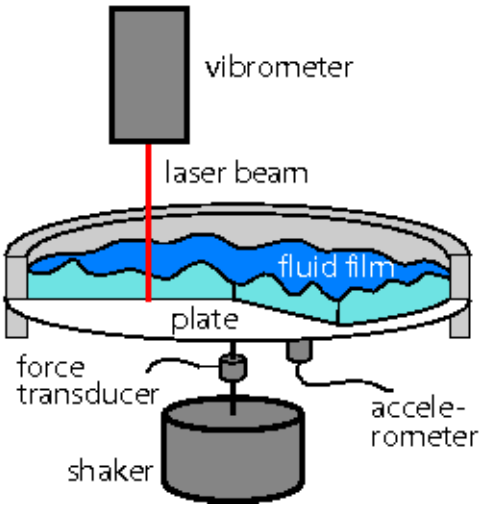

Fig. 4. Experimental configuration.

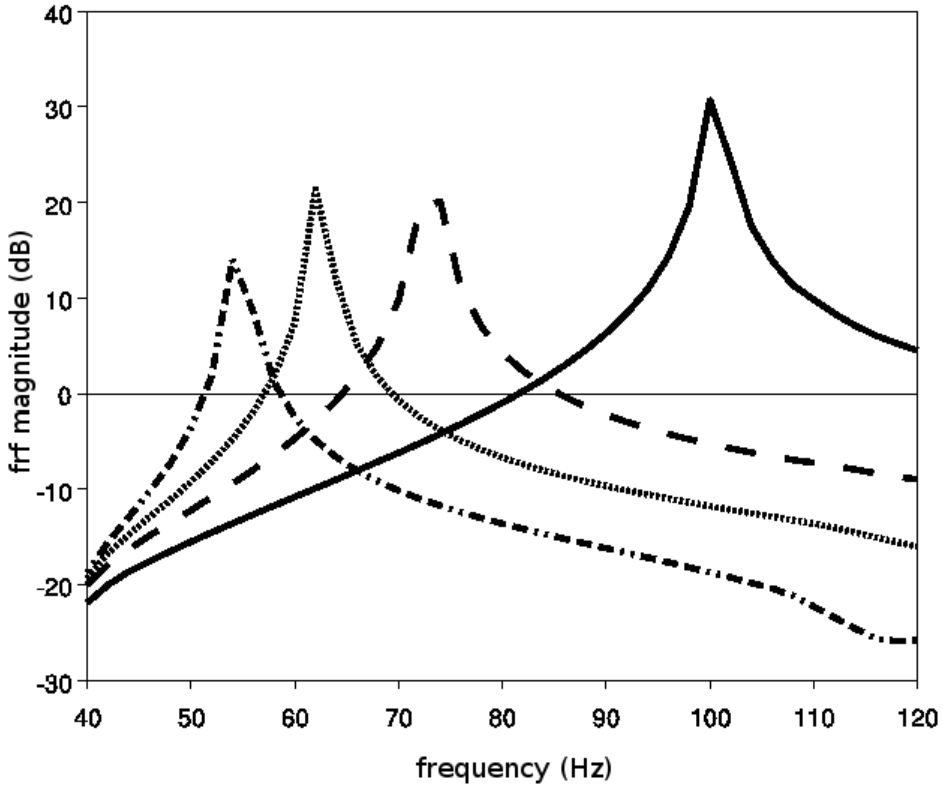

Fig. 5. Influence of the water level on the magnitude of the frequency response functions (acceleration/force): continuous line, bare plate ; dashed line, $\tilde{\rho} = 0.88$ (film thickness 4.6 mm) ; dotted line, $\tilde{\rho} = 1.53$ (film thickness 8.0 mm) ; dashed dotted line $\tilde{\rho} = 2.54$ (film thickness 13.3 mm). Acceleration at the center of the plate : 12.7 m s^{-2}.

.

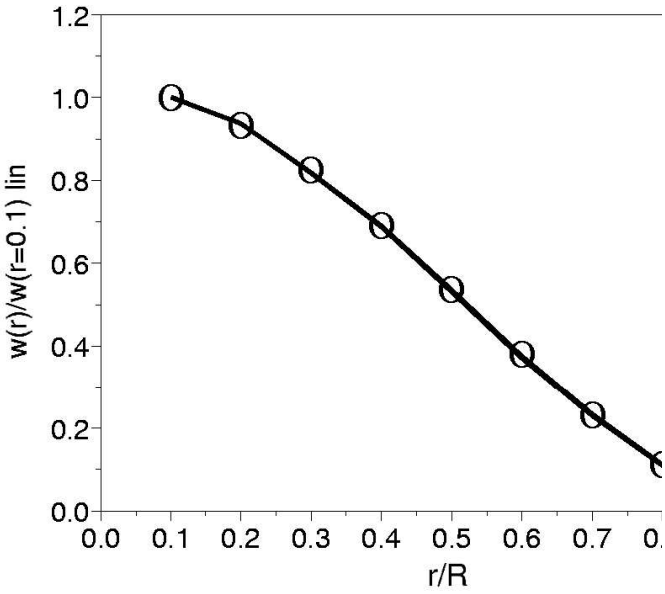

Fig. 6. Experimental mode shape of the plate along a radius near the first resonance of the bare plate, obtained by using laser velocimetry (continuous line) compared to the theoretical results (circles). Acceleration at the center of the plate : 19 m s^{-2}.

.

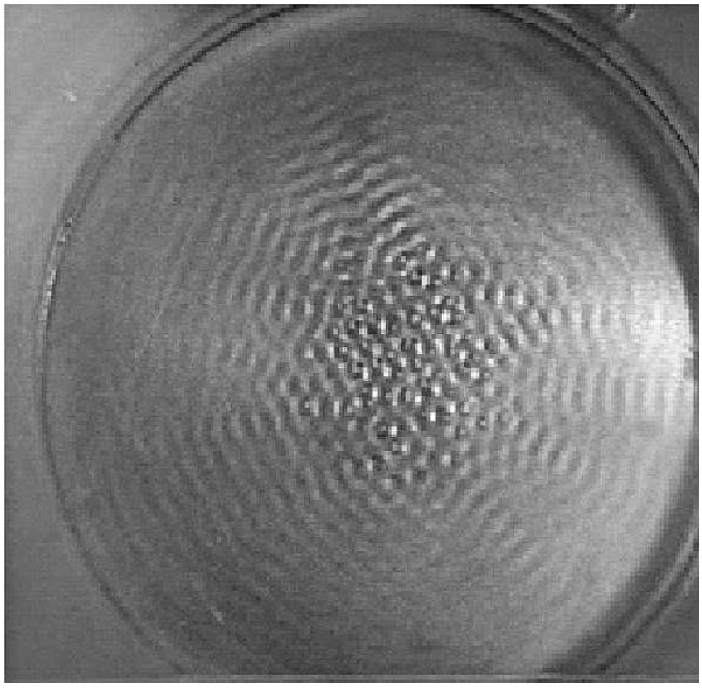

Fig. 7. Stationary waves at the fluid-air interface (top view of the plate). Acceleration at the center of the plate : 12.7 m s^{-2}

.

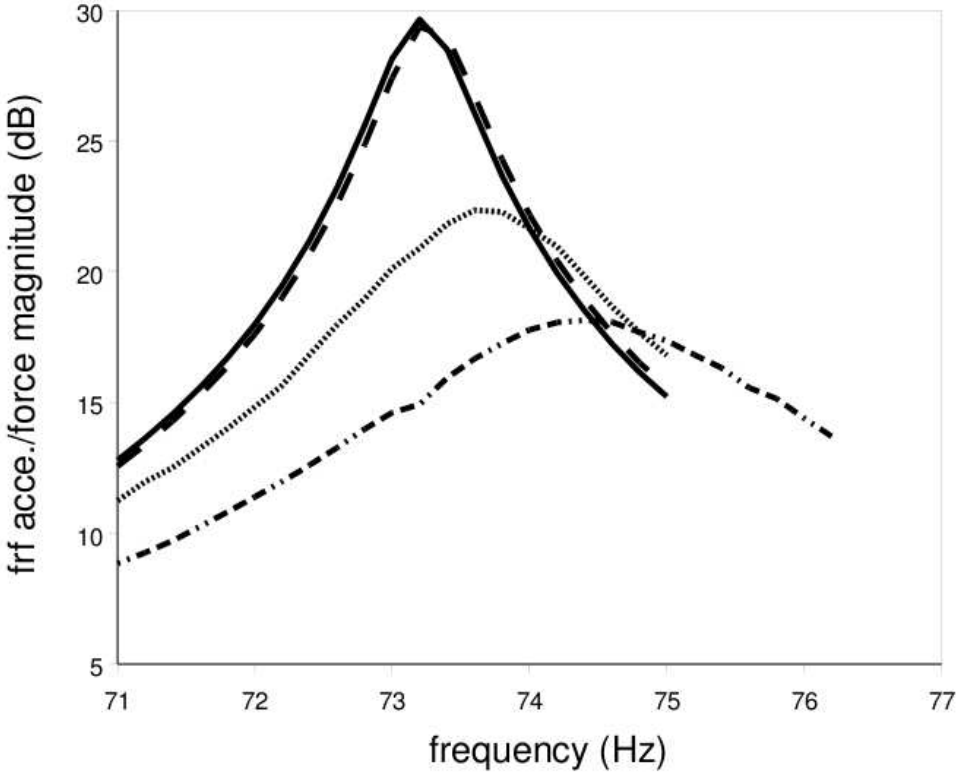

Fig. 8. Influence of the amplitude of the acceleration (measured at the center of the plate) on the frequency response function (accelerometer/force) of water added mass for a water level of 0.0046 m $\tilde{\rho} = 0.88$: continuous line, 3.16 m s^{-2} ; dashed line, 6.32 m s^{-2} ; dotted line, 12.7 m s^{-2} ; dashed dotted line, 25.3 m s^{-2}.

.

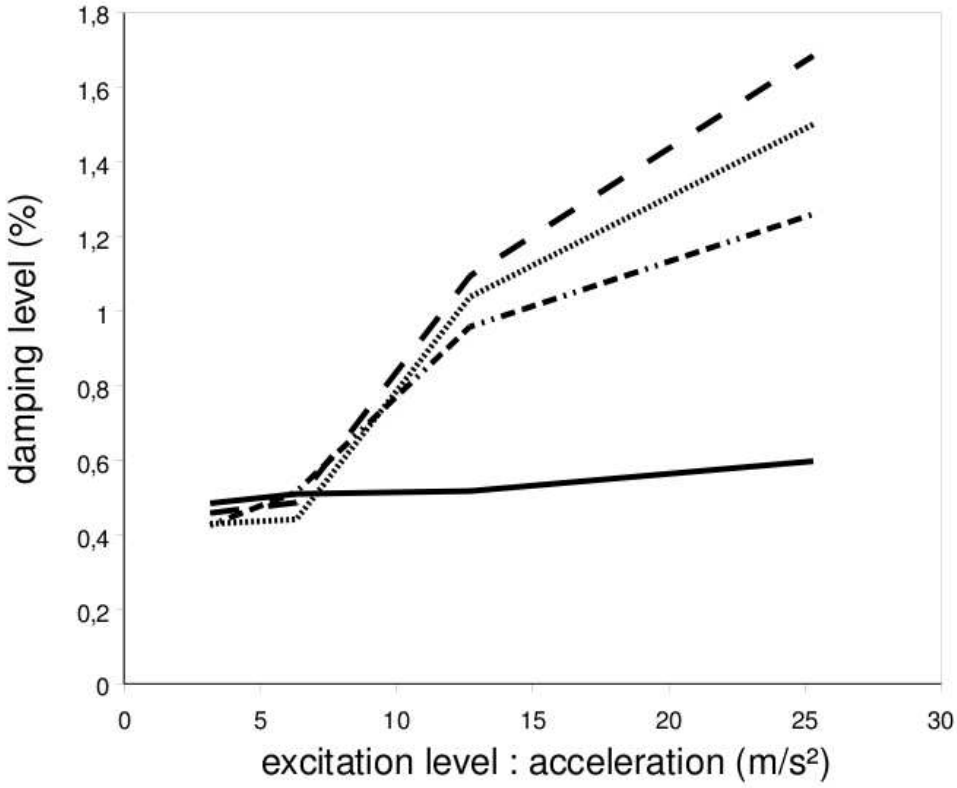

Fig. 9. Influence of the amplitude of the acceleration on the frequency response function of water added mass (accelerometer/force) for several water levels: continuous line, 0.0 m ; dashed line, 4.6 mm ; dotted line, 8.0 mm ; dashed dotted line, 13.3 mm.

.

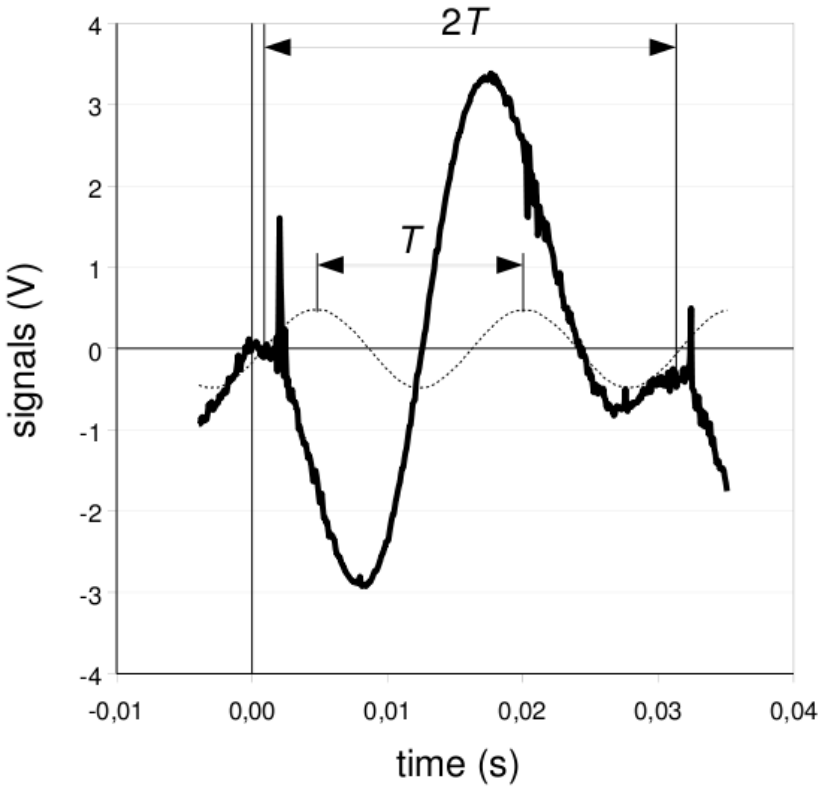

Fig. 10. Signals (V) of the apparent velocity of the plate measured through the fluid: the period of the velocity signal is twice the period of the acceleration signal (bold continuous line ; 1V=0.025 m s^{-1} ; maximum apparent velocity of the plate : 0.0875 m s^{-1}) and the acceleration of the plate (dotted line ; 1V=31.6 m s^{-2} ; maximum velocity of the plate : 0.039 m s^{-1}) ; water level 0.0046 m ; $\tilde{\rho} = 0.88$; frequency of excitation 65 Hz.

.

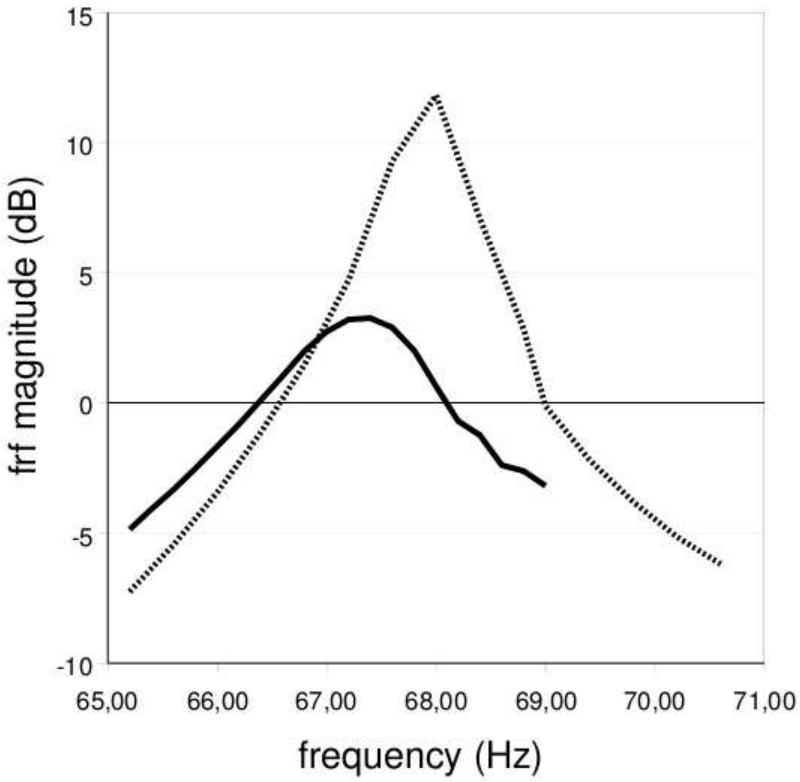

Fig. 11. Influence of the viscosity on the frequency response function (accelerometer/force) for an added mass of $\tilde{\rho} = 1.02$: continuous line, water (film thickness 5.3 mm) ; dotted line, oil (film thickness 7.2 mm). Acceleration at the center of the plate : 16.75 m s^{-2}

.

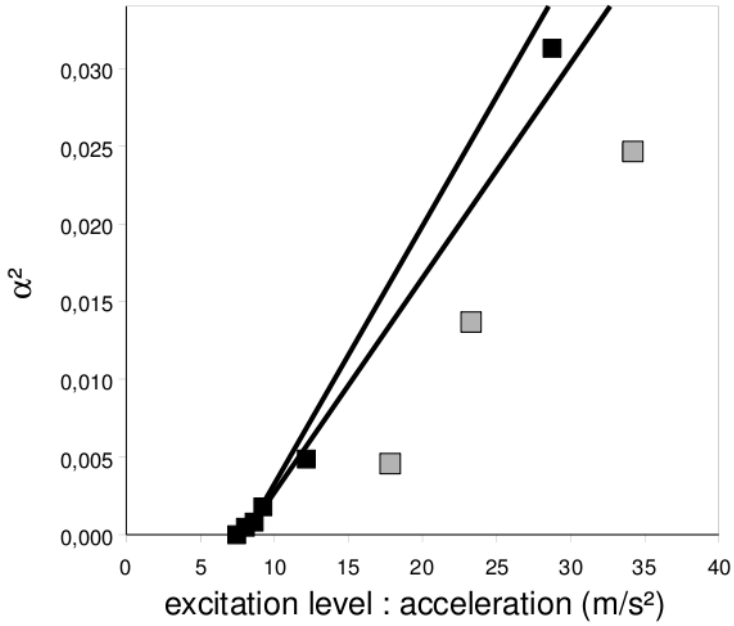

Fig. 12. Experimental evolution of the dimensionless oscillation amplitude $\alpha = A/h$ with the acceleration above the threshold for a given frequency (75 Hz) for water. The two lines corresponds to the uncertainty with a confidence of 95% of the mean square line which fits the datas.

.

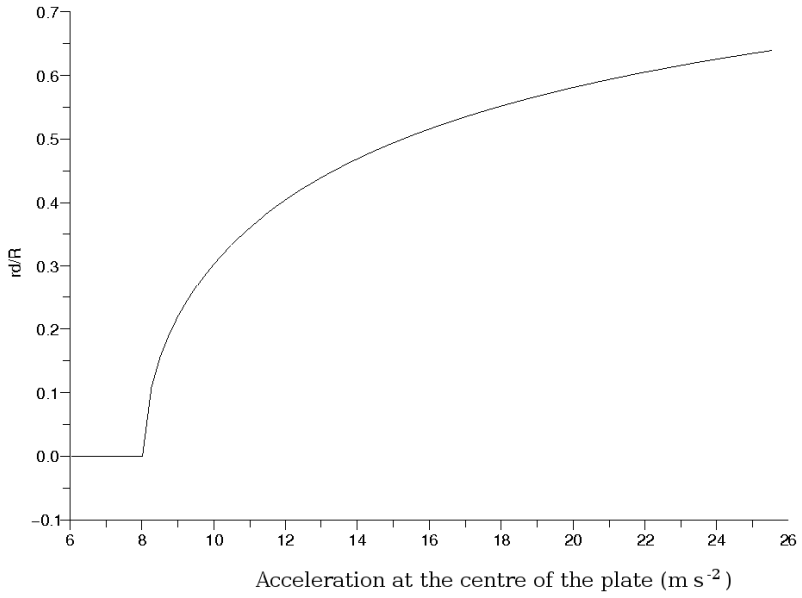

Fig. 13. Evolution of the radius of the instability area with the acceleration at the center of the plate $W_a(0,0)$.

.

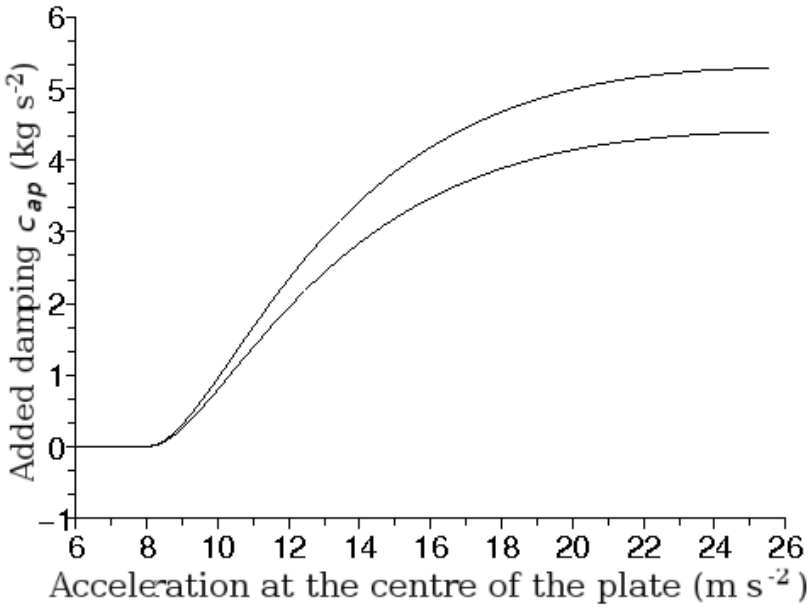

Fig. 14. The evolution of the damping coefficient added by the fluid to the structure with the acceleration at the center of the plate $W_a(0,0)$. The uncertainties on the measurement of the water waves induce two curves of added damping coefficient with 95% of confidence.

.

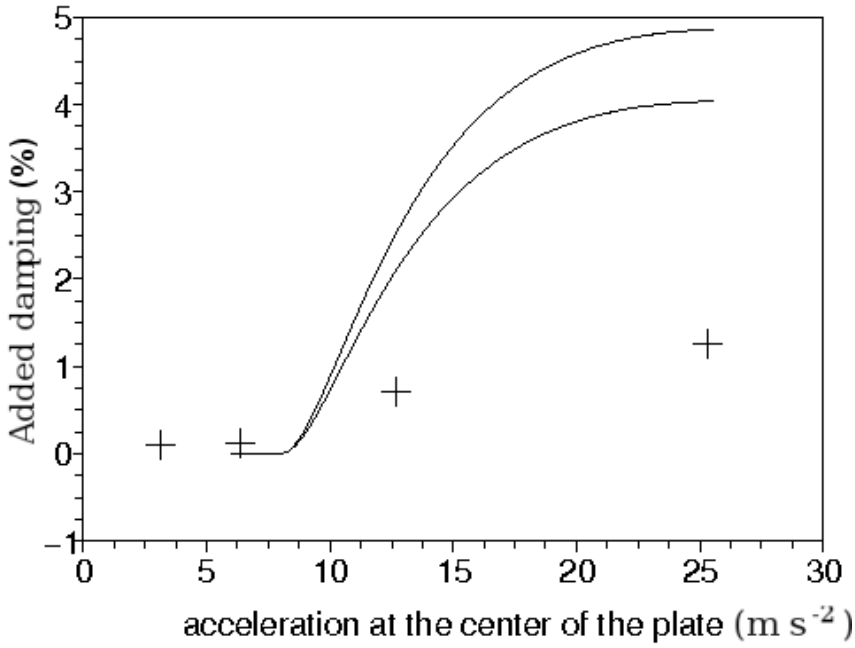

Fig. 15. Evolution of the damping ratio added by the fluid versus the acceleration at the center of the plate $\omega^2 W(0,0)$: theoretical values (between the two line: the uncertainties on the measurement of the water waves induce two curves of dimensionless damping with 95% of confidence), experimental values (crosses)

.

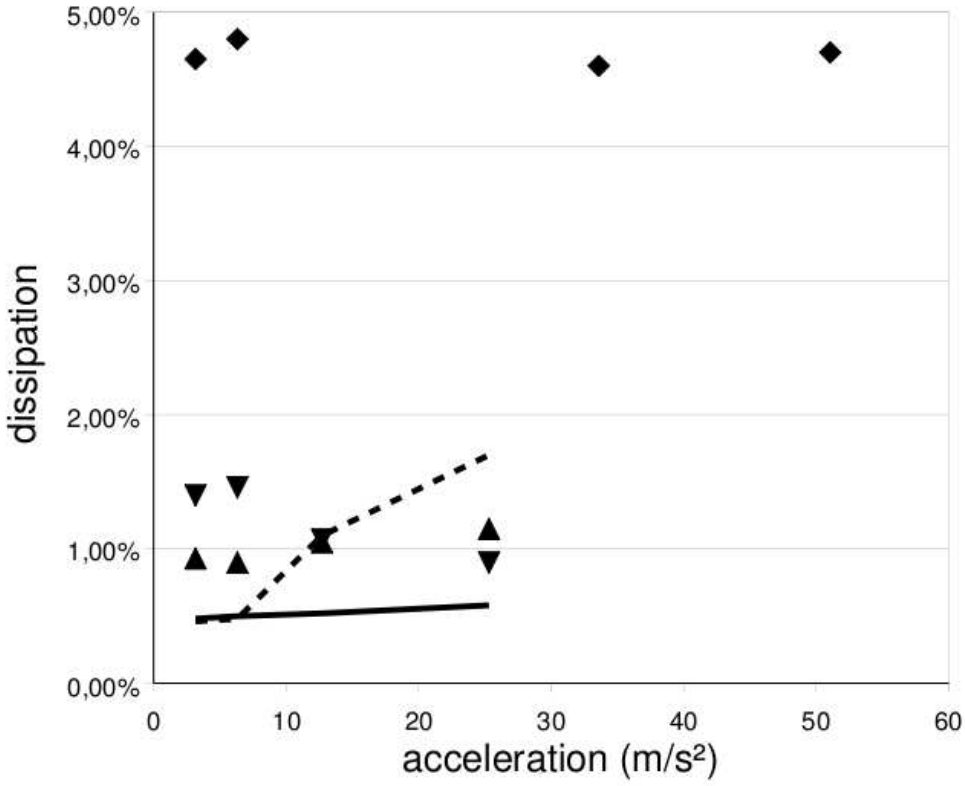

Fig. 16. Influence of the amplitude of the excitation on the damping: bare plate (continuous line) ; viscous treatment (diamond) ; foams (triangle down: Bulpren ; triangle up: NCF2) ; water (dotted line) level 4.6 mm.

.

.

List of Tables

diameter	$d = 0.290$ m
thickness	$e = 0.001$ m
material	aluminum
density (with air loading)	$\rho_s = 5230$ kg m^{-3}
Young Modulus	$E = 7\,10^{10}$ Pa
Poisson coefficient	$\nu_p = 0.3$

Table 1

Characteristics of the plate.

.

	NCF2	Bulpren
thickness (mm)	20.17	31
air flow resistivity (kN m^{-4} s)	75	4.8
density (kg m^3)	59	27.4
porosity	0.97	0.98
Young modulus at 5 Hz (MPa)	285	180
loss factor at 5 Hz	0.128	0.140
Poisson ratio	0.3	0.3

Table 2

Material properties of tested foams.

.